INTERNATIONAL JOURNAL OF ROBUST AND NONLINEAR CONTROL

Int. J. Robust Nonlinear Control 2002; **00**:1–6 *Prepared using* rncauth.cls *[Version: 2002/11/11 v1.00]*

Deployment algorithms for a power-constrained mobile sensor network

Andrew Kwok[1,*], Sonia Martínez[1]

[1] *University of California at San Diego*

Department of Mechanical and Aerospace Engineering

9500 Gilman Drive La Jolla, CA 92093-0411

SUMMARY

This paper presents distributed coverage algorithms for mobile sensor networks in which agents have limited power to move. Rather than making use of a constrained optimization technique, our approach accounts for power constraints by assigning non-homogeneously time-varying regions to each robot. This leads to novel partitions of the environment into limited-range, generalized Voronoi regions. The motion control algorithms are then designed to ascend the gradient of several types of Locational Optimization functions. In particular, the objective functions reflect the global energy available to the group and different coverage criteria. As we discuss in the paper, this has an effect on limiting each agent's velocity to save energy and balance its expenditure across the network. Copyright © 2002 John Wiley & Sons, Ltd.

KEY WORDS: Sensor network deployment, motion coordination, cooperative control

*Correspondence to: University of California at San Diego

Department of Mechanical and Aerospace Engineering

9500 Gilman Drive La Jolla, CA 92093-0411

1. Introduction

Mobile and static sensor networks hold the promise to impact a large number of applications for exploration, environmental monitoring, safety and recovery operations. It is envisioned that next network generations will make use of small low power mobile devices that operate in a distributed manner [1]. Due to their modest sizes and weights, these systems will have limited resources to divide between communication, computation and motion sub-capabilities. In this way, power management becomes a crucial issue for these systems.

One key area of interest regarding mobile sensor networks is deployment to maximize coverage, see for instance [2, 3, 4] and references therein. The ability to dynamically adjust to changes such as agent failure or target acquisition give mobile networks an advantage over static ones. Unfortunately, a drawback to mobile networks is that of increased power consumption.

Power-aware algorithms have been the subject of extensive research in static sensor networks and mobile middleware, see [5, 6]. However, limited work on power constraints and deployment has been done in the multi-vehicle sensor network field. The work of [7] and [8] utilize ordinary Voronoi diagrams and a discrete algorithm to show convergence through simulations. Energy considerations enter in their work as total distance traveled until convergence. Another related result from [9] considers a network of agents performing scan lines over a region of interest with energy and time constraints in mind. More involved vehicle energy dynamics are considered in that work, and they address the relevant problem of speed management as well as optimizing the number of agents necessary to provide adequate coverage in their deployment scheme.

This paper presents an alternative approach to the distributed deployment problem of mobile

sensor networks in which agents have limited energy budgets to move. To account for this, we design algorithms that limit the maximum distance an agent can travel by a dynamically-changing energy radius. This leads to a novel partition of the environment into limited-range, generalized Voronoi regions that produces a more balanced region assignment. Our algorithms seek to maximize objective functions involving: (i) the quantity of coverage as defined by area, and (ii) the quality of coverage as defined by standard Locational Optimization theory [10].

The new partitions become very useful in order to obtain gradient algorithms that guarantee local maximization of the objective functions. To do so, we consider a kinematic energy expenditure model for each agent. The maximization of the objective functions will then require that agents tune their speed as prescribed by the gradient information. The analysis provided here extends and merges previous work in [11], where coverage algorithms for agents with homogeneous, static sensor ranges is studied, and in [12], where energy partitions for coverage are initially explored disregarding energy constraints on mobility. More precisely, the work in [11] is extended to heterogeneous sensing radii that change dynamically as agents spend energy.

We include simulations of each algorithm that show that the corresponding objective functions are maximized. In particular we observe that the basic area-maximizing algorithm may lead to situations where coverage remains constant and yet agents expend energy. To avoid this, we modify our algorithm in two ways: (i) we limit further how fast agents can move but still maximizing the area covered, and (ii) we redesign the algorithms so that a mixed area-centroidal objective coverage function is maximized.

The paper is organized as follows. In Section 2 we define the problem and present the objective functions that we would like to maximize. In Section 3, we present the

partition necessary to implement the maximization of the functions in a distributed way with energy constraints. We analyze the objective functions in Section 4, and present their gradient directions. Section 5 introduces a common gradient ascent algorithm with guaranteed performance to apply to each case. In addition, we address some issues that may arise with such flows. We present simulation results in Section 6 and discuss the performance of the algorithms. Finally we point out lines for future research in Section 7.

2. Notation and Problem Definition

Let Q be a convex polytope in $\mathbb{R}^N$ including its interior, and let $\|\cdot\|$ denote the Euclidean norm. We will use $\mathbb{R}_{\geq 0}$ to denote the set of positive real numbers. A map $\phi : Q \to \mathbb{R}_{\geq 0}$, or a *distribution density function*, will represent a measure of a priori known information distinguishing zones of Q which are more important than others. Equivalently, we consider Q to be the bounded support of the function ϕ. We denote the interior of a set, $S \subset \mathbb{R}^N$, as $\mathrm{Int}\,(S)$, its complement as S^C, and its boundary as ∂S. The cardinality of S is denoted as $|S|$. A partition of Q is a collection of sets, $\mathcal{A} = \{A_1, \ldots, A_n\}$, such that: (i) $\mathrm{Int}\,(A_i) \cap \mathrm{Int}\,(A_j) = \emptyset$ for all $i \neq j$ and, (ii) $\bigcup_{i=1}^n A_i = Q$.

Let $P = (p_1, \ldots, p_n) \in Q^n$ be the *location of n sensors*, each moving in Q. We interchangeably refer to the elements of the network as sensors, agents, vehicles, or robots. The sensors have an associated energy content E_i such that $0 \leq E_i \leq E_{\max}$, for all $i \in \{1, \ldots, n\}$. As agents move, their energy reserve will change. We propose the following agent dynamics in the augmented state $(p_i, E_i) \in Q \times \mathbb{R}_{\geq 0}$:

$$\dot{p}_i = u_i\,, \qquad \dot{E}_i = -g_i(\|\dot{p}_i\|)\,, \tag{1}$$

where $\dot{p}_i$ denotes the velocity of agent i such that $\|\dot{p}_i\| \in [0, v_{\max}]$, u_i is the control input, and $g_i \colon [0, v_{\max}] \to \mathbb{R}_{\geq 0}$ is any increasing function such that $g_i(x) = 0$ only at $x = 0$. Intuitively, $g_i(x)$ captures the fact that energy expenditure increases as velocity increases. We will suppose that $g_i = g$ for all $i \in \{1, \ldots, n\}$.

We wish to deploy the robots to maximize a performance metric that quantifies coverage and employs the guaranteed travel ranges for agents. In the most general sense, and motivated by a Locational Optimization approach [10], we seek to maximize a general objective function

$$\mathcal{H}(P, W) = \int_Q \max_{i \in \{1,\ldots,n\}} f_i(d_{w_i}(q, p_i))\phi(q)dq \,, \tag{2}$$

where $f_i \colon \mathbb{R} \to \mathbb{R}$ is a non-increasing function associated with the sensing quality of agent i, and $d_{w_i} \colon \mathbb{R}^N \times \mathbb{R}^N \to \mathbb{R}$ is some metric function weighted by a scalar $w_i \in \mathbb{R}$, for all $i \in \{1, \ldots, n\}$. These scalars will be related to the travel ranges for each agent. Depending on the interpretation of coverage, $\mathcal{H}$ can be further specialized as we see in the following.

2.1. Energy-aware coverage

In [2], the metric $d_{w_i}(q, p_i)$ in (2) was taken to be the square of the Euclidean distance. Thus, $d_{w_i}(q, p_i) = \|q - p_i\|^2$ and there is no weight associated with this metric. We propose a natural extension of the results of [2] by considering a metric somehow weighted by the energy content of each vehicle. As will be explained in a later section, we will choose

$$d^e_{E_i}(q, p_i) = \|q - p_i\|^2 - E_i^2 \,, \tag{3}$$

$$d^m_{E_i}(q, p_i) = \frac{1}{E_i^2}\|q - p_i\|^2 \,, \tag{4}$$

called, respectively, the *power-weighted metric* and the *multiplicatively-weighted metric*, see [10].

By modifying the Euclidean distance as in (3), (4), notice that a point q appears farther away if the energy level of an agent is lower. The associated Locational Optimization function for $f_i(x) = -x$, becomes:

$$\mathcal{H}_{ea}(P, W) = \int_Q \max_{i \in \{1,\ldots,n\}} \{-d_{w_i}(q, p_i)\} \phi(q) dq \,. \tag{5}$$

2.2. Energy-limited coverage

We now formulate the notion of *guaranteed travel range*, the set of points that an agent can reach if it travels in a straight line at any fixed velocity $\|\dot{p}_i\| = v_i \in (0, v_{\max}]$ before running out of energy. Without loss of generality, assume $p_i(t_0) = 0$ and $E_i(t_0) > 0$ at some initial time t_0. We wish to find

$$R = \min_{v_i \in (0, v_{\max}]} \|p_i(T)\| \,, \tag{6}$$

where $T > 0$ satisfies $E_i(T) = 0$. From (1), and for a constant velocity different from zero, we have that $E_i(t) - E_i(t_0) = -g(v_i)(t - t_0)$, and so

$$T = \frac{E_i(t_0)}{g(v_i)} + t_0 \,. \tag{7}$$

Integrating $\dot{p}_i$ from (1), we get $p_i(t) = (t - t_0)v_i$. From (6) and (7), we obtain

$$R = \min_{v_i \in (0, v_{\max}]} \left\| \frac{E_i(t_0) v_i}{g(v_i)} \right\| \,. \tag{8}$$

Note that if $g(x)$ is a polynomial satisfying $g(0) = 0$, then (8) is well-defined. In addition, for any other velocity profile $\tilde{v}_i(t)$ along a straight line path, the resulting travel range $\tilde{R}$ is such that $\tilde{R} \geq R$.

For simplicity, we assume the following energy dynamics for each vehicle:

$$\dot{E}_i = -\|\dot{p}_i\|^2 = -\|u_i\|^2 \,, \quad i \in \{1, \ldots, n\} \,. \tag{9}$$

Without loss of generality, we can let $v_{\max} = 1$, and from (8), the guaranteed travel range is $R = E_i(t_0)$.

If we interpret coverage to be the set of all reachable points in Q, then under the previous assumptions, the range of an agent $i \in \{1, \ldots, n\}$ is equal to the amount of energy E_i that it has. Let $B_i = B(p_i, E_i)$ be a closed ball centered at p_i with radius E_i and let $S_i = B_i \setminus \mathrm{Int}\,(B_i)$ be a sphere centered at p_i with radius E_i. We will let $\mathcal{R} = Q \cap \bigcup_{i=1}^{n} B_i$ denote the set of all covered points by the group of agents. We now introduce various objective functions with the energy constraint in mind.

Area Coverage. The simplest problem to solve given the energy-limited constraint is to maximize area covered. Therefore, we can set $f_i(x) = 1_{[0,E_i]}(x)$ (i.e., the indicator function of the set $[0, E_i]$) and $d_{w_i}(q, p_i) = \|q - p_i\|$. Under these assumptions, the general objective function (2) becomes:

$$\mathcal{H}_a(P, E) = \int_Q \max_{i \in \{1,\ldots,n\}} 1_{[0,E_i]}(\|q - p_i\|)\phi(q)dq = \int_{\mathcal{R}} \phi(q)dq\,. \tag{10}$$

Centroidal Coverage. We can combine the energy-limited range with a typical objective function from Locational Optimization to obtain:

$$\mathcal{H}_c(P, E) = \int_{\mathcal{R}} \max_{i \in \{1,\ldots,n\}} \{-d_{E_i}(q, p_i)\}\phi(q)dq\,. \tag{11}$$

This has the interpretation of minimizing the mean distance from a point q to an agent at p_i.

Mixed Coverage. We can combine (10) and (11) to strike a balance between quantity of coverage and quality of coverage. We introduce two weights, κ_a, κ_c, to emphasize one over the other. The mixed coverage objective function is:

$$\mathcal{H}_m(P, E) = \kappa_a \mathcal{H}_a(P, E) + \kappa_c \mathcal{H}_c(P, E)\,. \tag{12}$$

Base Return. Another modification to the coverage objective function (10) would be to incorporate a "distance-from-home" cost. This addition has the practical interpretation that agents need to have enough energy to return to the base where they started. One implementation of such a constraint could have the following base-return objective function

$$\mathcal{H}_{br}(P,E) = \mathcal{H}_a(P,E) - \sum_{i=1}^{n} \rho(q_0, p_i, E_i)\,, \tag{13}$$

where the function ρ penalizes distance from some home point q_0. In applications where distance from home is a strict constraint, one can use $\rho(q_0, p_i, E_i) = \exp[\|q_0 - p_i\|^2 - E_i^2]$, $i \in \{1, \ldots, n\}$.

3. Limited-range, generalized Voronoi regions and associated proximity graphs

In order to come up with local deployment rules for each agent, it is convenient to assign different regions of the space to them. Similarly as in [11, 12], the regions of dominance should reflect each agent's ability to cover an area. These assignments will also define the graphs that determine the degree of decentralization of the proposed algorithms. In this section we introduce novel partitions of $\mathcal{R}$, $\mathcal{D}^e = \{D_1^e, \ldots, D_n^e\}$ and $\mathcal{D}^M = \{D_1^m, \ldots, D_n^m\}$, based on energy motion constraints.

3.1. Global partitions determined from the intersection of spheres

Let us consider a configuration like the one shown in Figure 1 where every two spheres S_i, S_j have an intersection $S_i \cap S_j$ at two points. A possibility is to define D_i^e as the region given by the intersection of B_i with halfplanes, $H(p_i, p_j)$, $\forall\, i \neq j$. The halfplanes $H(p_i, p_j)$ contain p_i and have as a boundary the line passing through the points in $S_i \cap S_j$. Using a halfplane that contains all such points provides a computationally convenient method of assigning regions of

dominance. The halfplanes that define boundaries between two regions can also be thought of as the convex hull of $S_i \cap S_j$ in the case where $|S_i \cap S_j| > 1$. This intuitive construction can be extended to cases where the spheres S_i, S_j are tangent or have zero intersection through the observation provided in the following lemma.

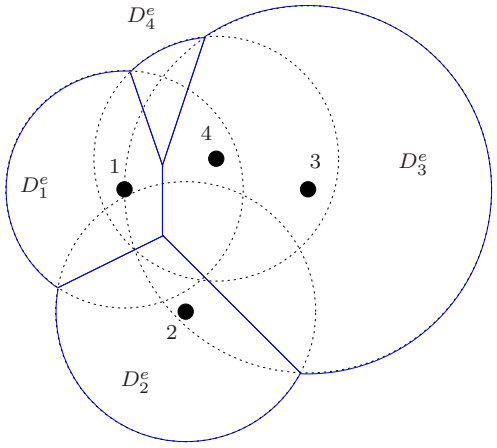

Figure 1. Proposed partition of $\mathcal{R}$. The individual spheres are shown in dotted lines, along with the boundaries of D_i^e in solid lines.

Lemma 1. *The intersection of spheres S_i generated by n agents with positions p_i and energies E_i for all $i \in \{1, \ldots, n\}$ induces a natural global partition of $\mathbb{R}^N$ which is the power-weighted Voronoi diagram (PWVD), $\mathcal{V}^e = (V_1^e, \ldots, V_n^e)$,*

$$V_i^e = \{q \in \mathbb{R}^N \mid \|q - p_i\|^2 - E_i^2 \leq \|q - p_j\|^2 - E_j^2\}\,, \tag{14}$$

for all $i \in \{1, \ldots, n\}$.

Proof: Now we examine two intersecting spheres in order to formulate some expression for the boundary points,

$$\mathrm{co}(S_i \cap S_j) = \{q \in \mathbb{R}^N \mid \|q - p_i\|^2 - E_i^2 = \|q - p_j\|^2 - E_j^2,\, \forall\, i \neq j\}\,.$$

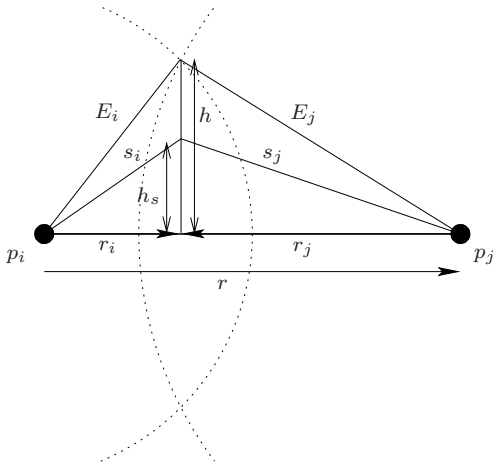

Figure 2. Diagram for the derivation of the Voronoi boundary location.

Examining Figure 2, we can see that:

$$\begin{cases} r_i - r_j = r\,, \\ E_i^2 - \|r_i\|^2 = E_j^2 - \|r_j\|^2\,. \end{cases}$$

Note that r_i, r_j and r are vectors, so if $E_j > \|r\|$ in Figure 2, then the above relationships still hold. We solve for r_j in the first equation and substitute into the second:

$$E_i^2 - \|r_i\|^2 = E_j^2 - \|r_i - r\|^2 = E_j^2 - \|r_i\|^2 + 2r^T r_i - \|r\|^2\,.$$

Since r and r_i point in the same direction, their inner product is the product of their individual magnitudes,

$$r^T r_i = \|r\|\|r_i\| = \frac{E_i^2 - E_j^2 + \|r\|^2}{2} \quad \Rightarrow \quad r_i = \frac{E_i^2 - E_j^2 + \|r\|^2}{2\|r\|}\frac{r}{\|r\|}\,.$$

Note that even though we considered the intersection as in Figure 2, we can arrive at a similar conclusion with a different type of intersection (i.e., one leading to an obtuse triangle.)

We now return to the case illustrated in Figure 2. Points along each boundary $\mathrm{co}(S_i \cap S_j)$ satisfy

$$\begin{cases} \|r_i\|^2 + \|h_s\|^2 = \|s_i\|^2 \,, \\ \|r_j\|^2 + \|h_s\|^2 = \|s_j\|^2 \,. \end{cases}$$

Subtracting the two equations, we get

$$\begin{aligned} \|s_i\|^2 - \|s_j\|^2 &= \|r_i\|^2 - \|r_j\|^2 = \|r_i\|^2 - \|r_i - r\|^2 \\ &= \|r_i\|^2 - \|r_i\|^2 + 2r_i^T r - \|r\|^2 \\ &= 2\frac{E_i^2 - E_j^2 + \|r\|^2}{2\|r\|}\|r\| - \|r\|^2 = E_i^2 - E_j^2 \,. \end{aligned}$$

This gives our final result,

$$\|s_i\|^2 - E_i^2 = \|s_j\|^2 - E_j^2 \,.$$

In other words, points $q \in \mathrm{co}(S_i \cap S_j)$ satisfy $\|q - p_i\|^2 - E_i^2 = \|q - p_j\|^2 - E_j^2$. Note that a set of points, $q \in \mathbb{R}^N$ that satisfy this property, exists regardless of whether or not S_i, S_j intersect. In fact, this boundary requirement is found in [10] as the defining property of the *power-weighted Voronoi partition*, with a weighting factor of E_i^2 for each generating point p_i.

■

It can be seen [10] that the boundary of a PWVD region is made of straight lines in two dimensions, or (hyper-) planes in higher dimensions. Thus, each of the V_i^e is convex. By construction, this indeed creates a partition of $\mathbb{R}^N$. According to [10], generator points p_i may fall outside their corresponding region V_i^e. See Figure 3 for an illustration of the PWVD, $\mathcal{V}^e$.

From now on, we adopt the following nomenclature. When two Voronoi regions V_i^e and V_j^e are adjacent (i.e., they share an edge), p_i is called a (power-metric) *Voronoi neighbor* of p_j. The set of indices of the power-metric Voronoi neighbors of p_i is denoted by $\mathcal{N}_i^e$. We define the (i, j)

face as $\Delta_{ij}^e = V_i^e \cap V_j^e$. Note also that a definition for $\mathcal{N}_j^e$ may be obtained from the dual of the PWVD, the power-weighted Delaunay graph, $\mathcal{G}_{\mathrm{D}}^e$. The graph $(P, E) \to \mathcal{G}_{\mathrm{D}}^e = (P, \mathcal{E}_{\mathrm{D}}^e(P, E))$ is a type of proximity graph (see [11]) consisting of the vertices P and the edges $\mathcal{E}_{\mathrm{D}}^e(P, E)$ such that

$$\mathcal{E}_{\mathrm{D}}^e(P, E) = \{(p_i, p_j) \in P \times P \setminus \mathrm{diag}(P \times P) \mid V_i^e \cap V_j^e \neq \emptyset\}.$$

In this way, we can define the neighbors of p_i in $\mathcal{G}_{\mathrm{D}}^e$ as:

$$\mathcal{N}_i^e = \{p_j \in P \mid (p_i, p_j) \in \mathcal{E}_{\mathrm{D}}^e(P, E)\}. \tag{15}$$

An alternate global partition to $\mathcal{V}^e$ can be determined by the following considerations. Recall from Section 2 that if $v_i = v_j = v_{\max}$, then two agents must spend all of their energy to reach a point at the intersection of the energy spheres $S_i \cap S_j$. However, both agents do not spend a proportionately equal amount of energy to reach points along the interior of the boundary segments $\Delta_{ij}^e \cap B_i$. For this to be the case, the property that needs to be satisfied is $\frac{1}{E_i^2}\|q - p_i\|^2 = \frac{1}{E_j}\|q - p_j\|^2$. In fact, this corresponds to the *multiplicatively-weighted Voronoi diagram* (MWVD), $\mathcal{V}^M = \{V_1^m, \ldots, V_n^m\}$, such that:

$$V_i^m = \left\{ q \in \mathbb{R}^N \mid \frac{1}{E_i^2}\|q - p_i\|^2 \leq \frac{1}{E_j^2}\|q - p_j\|^2 \right\}, \quad i \in \{1, \ldots, n\}. \tag{16}$$

Thus, given $v_i = v_j = v_{\max}$, agents spend proportionately equal amounts of energy to reach boundary points, $\Delta_{ij}^M = V_i^m \cap V_j^m$. According to [10], for this type of partition, generator points p_i lie in their regions, which may not be convex, may have holes and be disconnected. The boundaries of these regions are composed of circular arcs. As in the power-weighted case (14), the MWVD induces its own multiplicatively-weighted Delaunay graph, $\mathcal{G}_{\mathrm{D}}^m$, with corresponding edges $\mathcal{E}_{\mathrm{D}}^m(P, E)$ and neighbors $\mathcal{N}_i^m$.

Figure 3 compares the power-weighted Voronoi partition with the multiplicatively-weighted one, when intersected with a convex polytope Q. Notice that the intersected regions of $\mathcal{V}^e$ are convex whereas the ones associated with $\mathcal{V}^m$ are not.

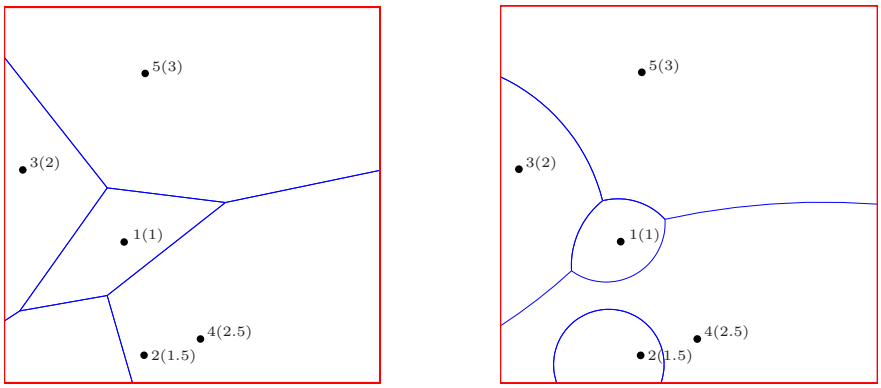

Figure 3. Comparison of the power-weighted (left) and multiplicatively-weighted (right) Voronoi diagrams. Energy contents are shown in parentheses. Observe that agent 2 is outside its region in the power-weighted case.

3.2. Limited-range partitions

Thus far, we have proposed two possible partitions of the entire space $\mathbb{R}^N$, (14) and (16). We now incorporate these two partitions with the limited range concept from Section 2.

In order to partition $\mathcal{R} = Q \cap \bigcup_{i=1}^{n} B_i$, we propose that each element of $\mathcal{D}^e = \{D_1^e, \ldots, D_n^e\}$ (resp. $\mathcal{D}^m = \{D_1^m, \ldots, D_n^m\}$) be defined as $D_i^e = Q \cap B_i \cap V_i^e$ (resp. $D_i^m = Q \cap B_i \cap V_i^m$), $i \in \{1, \ldots, n\}$. Agent regions of dominance, D_i^e (resp. D_i^m), will have boundaries that consist of Voronoi face segments $\Delta_{ij}^e \cap B_i \cap Q$ (resp. $\Delta_{ij}^m \cap B_i \cap Q$), boundary segments $\partial Q \cap B_i \cap V_i^e$ (resp. $\partial Q \cap B_i \cap V_i^m$), and energy radius arcs. We will refer to the union of all those arcs as $\text{Arcs}\,(D_i^e)$, which gives $\partial D_i^e = \bigcup_{j \in \mathcal{N}_i^e} \left(\Delta_{ij}^e \cap B_i\right) \cup (\partial Q \cap B_i \cap V_i^e) \cup \text{Arcs}\,(D_i^e)$ (resp. $\text{Arcs}\,(D_i^m)$

and $\partial D_i^m = \bigcup_{j\in\mathcal{N}_i^m} \left(\Delta_{ij}^m \cap B_i\right) \cup (\partial Q \cap B_i \cap V_i^m) \cup \mathrm{Arcs}\left(D_i^m\right)$). This proposed partition will also have a dual graph, the energy-limited Delaunay graph $\mathcal{G}_{\mathrm{LD}}^e = (P, \mathcal{E}_{\mathrm{LD}}^e(P,E))$ (resp. we have $\mathcal{G}_{\mathrm{LD}}^m$). The edge set is defined as

$$\mathcal{E}_{\mathrm{LD}}^e(P,E) = \{(p_i,p_j) \in P\times P \setminus \mathrm{diag}(P\times P) \mid D_i^e \cap D_j^e \neq \emptyset \,\mathrm{and}\, \|p_i - p_j\| \leq E_i + E_j\}\,.$$

This allows the definition of the set of neighbors,

$$\mathcal{N}_{i,\mathrm{LD}}^e = \{p_j \in P \mid (p_i,p_j) \in \mathcal{E}_{\mathrm{LD}}^e(P,E)\} = \{p_j \in P \mid D_i^e \cap D_j^e \neq \emptyset\}\,,$$

(resp. we have $\mathcal{N}_{i,\mathrm{LD}}^m$). In addition, the quantities M_i^e and C_i^e will denote the *mass* and *centroid* of either V_i^e or D_i^e. For example,

$$M_i^e = \int_{D_i^e} \phi(q)dq\,, \qquad C_i^e = \frac{1}{M_i^e}\int_{D_i^e} q\phi(q)dq\,.$$

It should be clear from the context whether M_i^e and C_i^e refer to the mass and centroid of V_i^e or D_i^e. (Resp. M_i^m and C_i^m refer to the mass and centroid of either V_i^m or D_i^m, i.e.: $M_i^m = \int_{D_i^m}\phi(q)dq$ and $C_i^m = \frac{1}{M_i^m}\int_{D_i^m} q\phi(q)dq$). In addition, we also define the *moment of inertia* of V_i^m or D_i^m as,

$$I_i^m = \int_{D_i^m} \|q-p_i\|^2\phi(q)dq\,.$$

As defined, it is not immediately clear that the collections $\mathcal{D}^e$ and $\mathcal{D}^m$ are partitions of $\mathcal{R}$. This is proved in the next theorem.

Theorem 2. *Let $\mathcal{D}^e = \{D_1^e,\ldots,D_n^e\}$ be a collection of sets with $D_i^e = B_i \cap V_i^e \cap Q$. Let $\mathcal{D}^M = \{D_1^m,\ldots,D_n^m\}$ with $D_i^e = B_i \cap V_i^e \cap Q$. Then, $\mathcal{D}^e$ and $\mathcal{D}^M$ are partitions of $\mathcal{R} = Q \cap \bigcup_{i=1}^n B_i$.*

Proof: We prove the result for $\mathcal{D}^e$, being the proof for $\mathcal{D}^m$ is analogous. Since the PWVD is a partition of $\mathbb{R}^N$, we have that $\mathrm{Int}\left(V_i^e\right) \cap \mathrm{Int}\left(V_j^e\right) = \emptyset$, for all $i \neq j$. Since $D_i^e = B_i \cap V_i^e \cap Q$,

then

$$\mathrm{Int}\,(D_i^e) = \mathrm{Int}\,(B_i \cap V_i^e) = \mathrm{Int}\,(B_i) \cap \mathrm{Int}\,(V_i^e) \cap \mathrm{Int}\,(Q)\ .$$

This implies that

$$\mathrm{Int}\,(D_i^e) \cap \mathrm{Int}\left(D_j^e\right) = \mathrm{Int}\,(B_i) \cap \mathrm{Int}\,(V_i^e) \cap \mathrm{Int}\,(B_j) \cap \mathrm{Int}\left(V_j^e\right) \cap Q = \emptyset\,.$$

Thus we have proved the first defining condition of a partition.

Now we must show $\bigcup_{i=1}^n D_i^e = Q \cap \bigcup_{i=1}^n B_i$. Expanding the left-hand side,

$$\bigcup_{i=1}^n D_i^e = \bigcup_{i=1}^n (V_i^e \cap B_i \cap Q) = Q \cap \bigcup_{i=1}^n B_i\,.$$

Thus it is sufficient to show $\bigcup_{i=1}^n (V_i^e \cap B_i) = \bigcup_{i=1}^n B_i$. Note also that

$$B_i = B_i \cap \left(V_i^e \cup (V_i^e)^C\right) = (B_i \cap V_i^e) \cup \left(B_i \cap (V_i^e)^C\right)\ .$$

Taking the union over all i,

$$\bigcup_{i=1}^n B_i = \left(\bigcup_{i=1}^n (B_i \cap V_i^e)\right) \cup \left(\bigcup_{i=1}^n \left(B_i \cap (V_i^e)^C\right)\right)\ .$$

If we show that $\left(B_i \cap (V_i^e)^C\right) \subset \bigcup_{j\neq i} D_j^e$, then we will have proved the requirement. Let $A_i = B_i \cap (V_i^e)^C$, and note that A_i may not be connected, however $\partial A_i = \bigcup_{j\in\mathcal{N}_i^e} (S_i \cap (V_i^e)^C) \cup (B_i \cap \Delta_{ij}^e)$.

Consider a point $q \in A_i$. Because $\mathcal{V}^e$ is a partition, there exists a $j_q \neq i$ such that,

$$\|q - p_j\|^2 - E_j^2 \geq \|q - p_{j_q}\|^2 - E_{j_q}^2\,, \qquad \forall j \neq j_q\,.$$

On the other hand $q \in A_i$ implies $\|q - p_i\|^2 \leq E_i^2$. Taking the first equation for $j = i$ and applying latest condition, we get

$$\|q - p_{j_q}\|^2 \leq \|q - p_i\|^2 - E_i^2 + E_{j_q}^2 \leq E_{j_q}^2\,.$$

This implies that $q \in D_{j_q}^e$. Since this argument is valid for any $q \in A_i$, we have that $A_i \subseteq \bigcup_{j\neq i} D_j^e$. ■

The two partitions of $\mathcal{R}$ yield similar results as can be seen in Figure 4. Generally speaking, the power-weighted partition $\mathcal{D}^e$ is a good approximation to the multiplicatively-weighted partition $\mathcal{D}^M$ if the agents are spaced far enough apart, or if the energy contents of neighbors are similar.

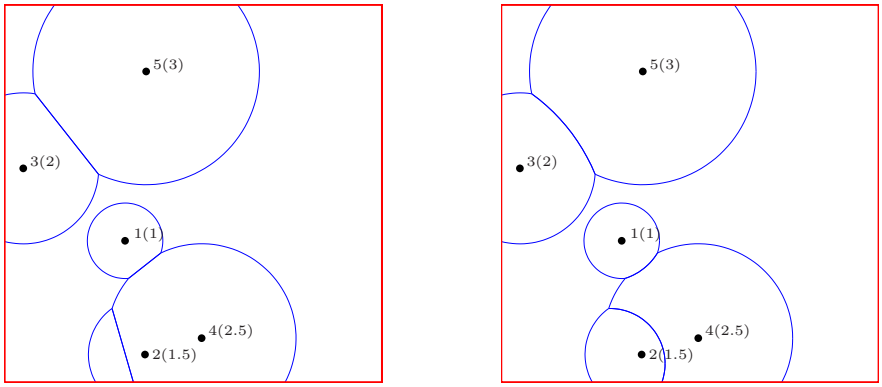

Figure 4. Comparison of the limited range power-weighted (left) and multiplicatively-weighted (right) partitions, for the same set of points from Figure 3. Energy contents are shown in parentheses.

4. Objective function gradient characterization

In this section we derive the gradient direction for each of the objective functions that we have introduced previously. These gradients define the proper direction of flow in order to optimize coverage. Before we begin, we restate the objective functions from Section 2 in a form that facilitates analysis.

The metric that generates the PWVD is the given metric (3). Similarly, the MWVD is determined from the metric (4). To better distinguish between the objective functions that use the PWVD metric and the MWVD metric, we will use $\mathcal{H}$ for the former and $\mathcal{J}$ for the latter.

We present the new forms of (5), (10), (11) (upon which the remaining objective functions (12) and (13) are based) using the PWVD here:

$$\mathcal{H}_{ea}(P,E) = \int_Q \max_{i\in\{1,\ldots,n\}} \{-d^e_{E_i}(q,p_i)\}\phi(q)dq = \sum_{i=1}^{n} \int_{V_i^e} -\left(\|q-p_i\|^2 - E_i^2\right)\phi(q)dq\,, \tag{17}$$

$$\mathcal{H}_{a}(P,E) = \int_{\mathcal{R}} \phi(q)dq = \sum_{i=1}^{n} \int_{D_i^e} \phi(q)dq\,, \tag{18}$$

$$\mathcal{H}_{c}(P,E) = \int_{\mathcal{R}} \max_{i\in\{1,\ldots,n\}} \{-d^e_{E_i}(q,p_i)\}\phi(q)dq = \sum_{i=1}^{n} \int_{D_i^e} -\left(\|q-p_i\|^2 - E_i^2\right)\phi(q)dq\,, \tag{19}$$

Through the use of the MWVD, we can rewrite the respective objective functions as:

$$\mathcal{J}_{ea}(P,E) = \int_Q \max_{i\in\{1,\ldots,n\}} \{-d^m_{E_i}(q,p_i)\}\phi(q)dq = \sum_{i=1}^{n} \int_{V_i^m} -\frac{1}{E_i^2}\|q-p_i\|^2\phi(q)dq\,, \tag{20}$$

$$\mathcal{J}_{a}(P,E) = \int_{\mathcal{R}} \phi(q)dq = \sum_{i=1}^{n} \int_{D_i^m} \phi(q)dq\,, \tag{21}$$

$$\mathcal{J}_{c}(P,E) = \int_{\mathcal{R}} \max_{i\in\{1,\ldots,n\}} \{-d^m_{E_i}(q,p_i)\}\phi(q)dq = \sum_{i=1}^{n} \int_{D_i^m} -\frac{1}{E_i^2}\|q-p_i\|^2\phi(q)dq\,. \tag{22}$$

Before computing the gradients we would like to note the following result.

Lemma 3. *The objective functions* (17)–(22) *are continuously differentiable with respect to* p_i *and* E_i*.*

Proof: This is a result of Proposition 1.6 in [11]. We have shown in Section 3 that the regions $V_i^e \cap Q$ and D_i^e are convex. Furthermore, these regions are formed by intersections of half-planes and balls, making them *piecewise smooth* as required in [11]. We also present ϕ to be the bounded support of Q, thus it is integrable over Q. This satisfies all the requirements of Proposition 1.6, so then the objective functions (17)–(19) are are continuously differentiable.

Even though regions of MWVD may not be star-shaped, each individual region $V_i^m \cap Q$ and D_i^m can be composed of a finite union of star-shaped sets, which makes such regions fall under the scope of the result from [11]. ■

We now state the gradient expressions for these functions.

Proposition 4. *Given the objective functions $\mathcal{H}_{ea}$, $\mathcal{H}_a$, $\mathcal{H}_c$, $\mathcal{H}_m$, and $\mathcal{H}_{br}$ based on* (17), (18), *and* (19), *and a general vector field $X = (X_1, \ldots, X_n)$ where $X_i = (X_{p_i}, X_{E_i}) : Q \times \mathbb{R} \to \mathbb{R}^N \times \mathbb{R}$ for all $i \in \{1, \ldots, n\}$, the Lie derivatives of $\mathcal{H}_{ea}$, $\mathcal{H}_a$, $\mathcal{H}_c$, $\mathcal{H}_m$, and $\mathcal{H}_{br}$ are*

$$\mathcal{L}_X \mathcal{H}_{ea} = \sum_{i=1}^{n} \left(2M_i^e (C_i^e - p_i)^T\right) X_{p_i} + 2E_i M_i^e X_{E_i}\,, \tag{23}$$

$$\mathcal{L}_X \mathcal{H}_a = \sum_{i=1}^{n} \left(\int_{\mathrm{Arcs}\left(D_i^e\right)} \phi(\gamma_i)[n^t(\gamma_i)]^T d\gamma_i \right) X_{p_i} + \left(\int_{\mathrm{Arcs}\left(D_i^e\right)} \phi(\gamma_i) d\gamma_i \right) X_{E_i}\,, \tag{24}$$

$$\mathcal{L}_X \mathcal{H}_c = \sum_{i=1}^{n} \left(2M_i^e (C_i^e - p_i)^T\right) X_{p_i} + \left(2E_i M_i^e\right) X_{E_i}\,, \tag{25}$$

$$\mathcal{L}_X \mathcal{H}_m = \kappa_a \mathcal{L}_X \mathcal{H}_a + \kappa_c \mathcal{L}_X \mathcal{H}_c\,, \tag{26}$$

$$\mathcal{L}_X \mathcal{H}_{br} = \mathcal{L}_X \mathcal{H}_a + \sum_{i=1}^{n} \left[2\rho(q_o, p_i, E_i)(q_0 - p_i)^T\right] X_{p_i} + \left[2E_i \rho(q_o, p_i, E_i)\right] X_{E_i}\,. \tag{27}$$

Proof: We will present the gradient calculations for $\mathcal{H}_{ea}$, $\mathcal{H}_a$, and $\mathcal{H}_c$ and note that the remaining gradients follow immediately from those results. We will use the conservation of mass law in [11] to differentiate the integral form of the objective functions,

$$\frac{d}{dx} \int_{\Omega(x)} \varphi(q, x) dq = \int_{\Omega(x)} \frac{d\varphi(q, x)}{dx} dq + \int_{\partial\Omega(x)} \varphi(\gamma, x) n^t(\gamma) \frac{\partial \gamma}{\partial x} dx\,,$$

where $n : \partial\Omega(x) \to \mathbb{R}^N$, $q \mapsto n(q)$ denotes the unit outward normal to $q \in \partial\Omega(x)$, and $\gamma : D \to \Omega(x)$, $D \subseteq \mathbb{R}^N$ denotes a parametrization of the family $\{\Omega(x) \subseteq \mathbb{R}^N \,|\, x \in D\}$ of star-shaped sets.

Energy-aware, (17). Applying this law,

$$\begin{aligned}\frac{\partial \mathcal{H}_{ea}}{\partial p_i} &= \frac{\partial}{\partial p_i}\sum_{j=1}^{n}\int_{V_j^e} -d_{E_j}^e(q,p_j)\phi(q)dq \\ &= \sum_{j=1}^{n}\int_{V_j^e} -\frac{\partial}{\partial p_i}d_{E_i}^e(q,p_i)\phi(q)dq + \sum_{j=1}^{n}\int_{\partial V_j^e} -d_{E_j}^e(\gamma_j,p_j)\phi(\gamma_j)n^t(\gamma_j)\frac{\partial \gamma_j}{\partial p_i}d\gamma_j \\ &= \int_{V_i^e} 2(q-p_i)\phi(q)dq + \int_{\partial V_i^e} -d_{E_i}^e(\gamma_i,p_i)\phi(\gamma_i)n^t(\gamma_i)\frac{\partial \gamma_i}{\partial p_i}d\gamma_i \\ &\quad + \sum_{j\in\mathcal{N}_i^e}\int_{\partial V_j^e} -d_{E_j}^e(\gamma_j,p_j)\phi(\gamma_j)n^t(\gamma_j)\frac{\partial \gamma_j}{\partial p_i}d\gamma_j\,.\end{aligned}$$

The final step comes from the fact that a small perturbation in position of one agent only affects the Voronoi boundaries of its neighbors $\mathcal{N}_i^e$. Note that over the set of shared boundaries, Δ_{ij}^e for $j \in \mathcal{N}_i^e$, the normal vectors are equal and opposite, $n^t(\gamma_i) = -n^t(\gamma_j)$. Therefore, the integrals along shared boundaries vanish, leaving the final result,

$$\frac{\partial \mathcal{H}_{ea}}{\partial p_i} = \int_{V_i^e} 2(q-p_i)\phi(q)dq = 2M_i^e(C_i^e - p_i)^T\,.$$

A similar analysis can be done for the energy derivative to obtain

$$\frac{\partial \mathcal{H}_{ea}}{\partial E_i} = \int_{V_i^e} 2E_i\phi(q)dq = 2E_iM_i^e\,.$$

Area coverage (18). We must calculate the expression for $\frac{\partial \mathcal{H}_a}{\partial p_i}$ and $\frac{\partial \mathcal{H}_a}{\partial E_i}$. Applying the conservation of mass law once again, we have

$$\begin{aligned}\frac{\partial \mathcal{H}_a}{\partial p_{i,k}} &= \frac{\partial}{\partial p_{i,k}}\sum_{j=1}^{n}\int_{D_j^e}\phi(q)dq = \sum_{j=1}^{n}\int_{D_j}\frac{\partial}{\partial p_{i,k}}\phi(q)dq + \sum_{j=1}^{n}\int_{\partial D_j^e}\phi(\gamma_j)n^t(\gamma_j)\frac{\partial \gamma_j}{\partial p_{i,k}}d\gamma_j \\ &= \int_{\partial D_i^e}\phi(\gamma_i)n^t(\gamma_i)\frac{\partial \gamma_i}{\partial p_{i,k}}d\gamma_i + \sum_{j\in\mathcal{N}_{i,\mathrm{LD}}^e}\int_{\partial D_j^e}\phi(\gamma_j)n^t(\gamma_j)\frac{\partial \gamma_j}{\partial p_{i,k}}d\gamma_j\,.\end{aligned}$$

Each region may have boundaries composed of circular arcs or planar faces. Over the set of shared faces Δ_{ij}^e, for all $j \in \mathcal{N}_{i,\mathrm{LD}}^e$, note that the normal vectors $n^t(\gamma_i) = -n^t(\gamma_j)$. Therefore, the integrals along shared boundaries vanish, leaving the integration over the arcs of D_i,

$$\frac{\partial \mathcal{H}_a}{\partial p_{i,k}} = \int_{\mathrm{Arcs}(D_i^e)}\phi(\gamma_i)n^t(\gamma_i)\frac{\partial \gamma_i}{\partial p_{i,k}}d\gamma_i\,. \tag{28}$$

From the definition of D_i^e, Arcs (D_i^e) are a fixed distance with respect to the generating point, p_i. In $\mathbb{R}^N$, let $\gamma_i(\Theta)$ be the parametrization of a particular point on the arc of D_i^e. Then,

$$\|\gamma(\Theta) - p_i\| = E_i \qquad \Rightarrow \qquad \frac{\partial}{\partial p_i}\|\gamma(\Theta) - p_i\| = 0$$

$$\|\gamma(\Theta) - p_i\|^{-1/2}(\frac{\partial \gamma}{\partial p_i} - I) = 0 \quad \Leftrightarrow \quad \frac{\partial \gamma}{\partial p_i} = I\,.$$

From (28) and the above result,

$$\frac{\partial \mathcal{H}_a}{\partial p_i} = \int_{\text{Arcs}\left(D_i^e\right)} \phi(\gamma_i)[n^t(\gamma_i)]^T d\gamma_i\,. \tag{29}$$

Similarly, we compute the derivative with respect to E_i:

$$\frac{\partial \mathcal{H}_a}{\partial E_i} = \int_{\text{Arcs}\left(D_i^e\right)} \phi(\gamma_i)\frac{\partial \gamma_i}{\partial E_i} n^t(\gamma_i) d\gamma_i\,.$$

Note that the boundary, γ_i, grows and shrinks proportional to the normal as E_i changes. Therefore, $\frac{\partial \gamma_i}{\partial E_i} = n^t(\gamma_i)$ and

$$\frac{\partial \mathcal{H}_a}{\partial E_i} = \int_{\text{Arcs}\left(D_i^e\right)} \phi(\gamma_i)\|n^t(\gamma_i)\|^2 d\gamma_i = \int_{\text{Arcs}(D_i)} \phi(\gamma_i) d\gamma_i\,. \tag{30}$$

Centroidal coverage (19). We apply the conservation of mass law in a similar way as the area coverage case. Note, however, that (3) has dependence on p_i, so we are left with

$$\frac{\partial \mathcal{H}_c}{\partial p_i} = -\int_{D_i^e} \frac{\partial}{\partial p_i} d^e_{E_i}(q, p_i) dq - \int_{\text{Arcs}\left(D_i^e\right)} d^e_{E_i}(\gamma_i, p_i) n^t(\gamma_i)\frac{\partial \gamma_i}{\partial p_i} d\gamma_i\,.$$

Using (3), the first term of the right hand side becomes $\int_{D_i^e} 2(q - p_i)\phi(q) dq$. Again, Arcs (D_i^e) are a fixed distance from p_i. Thus, the second term on the right hand side is

$$\int_{\text{Arcs}\left(D_i^e\right)} (E_i^2 - E_i^2)\phi(\gamma_i) n_k^t(\gamma_i) d\gamma_i = 0\,.$$

We can combine the above results to get:

$$\frac{\partial \mathcal{H}_c}{\partial p_i} = 2M_i^e(C_i^e - p_i)^T\,.$$

Similarly, we compute the derivative with respect to E_i:

$$\frac{\partial \mathcal{H}_c}{\partial E_i} = \int_{D_i^e} 2E_i \phi(q) dq = 2E_i M_i^e \,.$$

Putting these results together leads to (25) and (26).

Base-return (13). We have already computed the area coverage objective gradient, so all that remains is to compute

$$\frac{d}{dt}\left[\sum_{i=0}^{n} \rho(q_0, p_i, E_i)\right] = \sum_{i=0}^{n}\left[\frac{\partial \rho}{\partial p_i}\dot{p}_i + \frac{\partial \rho}{\partial E_i}\dot{E}_i\right] .$$

Suppose we would like to use $\rho(q_0, p_i, E_i) = -\exp[\|q_0 - p_i\|^2 - E_i^2]$. Then the respective derivatives would be

$$\frac{\partial \rho}{\partial p_i} = 2\exp[\|q_0 - p_i\|^2 - E_i^2](q_0 - p_i)^T \,,$$
$$\frac{\partial \rho}{\partial E_i} = 2E_i \exp[\|q_0 - p_i\|^2 - E_i^2] \,.$$

■

Remark 5. The area coverage result can be seen as a generalization of a limited sensing coverage problem in [11] for a network of heterogeneous sensors with different and constant sensing ranges R_i. The corresponding sensing range would satisfy $R_i = E_i^2$. However, since this sensing range is fixed, the Lie derivative will not have a second term involving energy. We would simply have

$$\frac{d\mathcal{H}_a}{dt} = \sum_{i=1}^{n}\left(\int_{\mathrm{Arcs}\left(D_i^e\right)} \phi(\gamma_i)[n^t(\gamma_i)]^T d\gamma_i\right)\dot{p}_i \,,$$

which extends the result found in [11]. •

Now we perform the same gradient analysis for the partitions based on the MWVD.

Proposition 6. *Consider the objective functions $\mathcal{J}_a$, $\mathcal{J}_c$, $\mathcal{J}_m$, and $\mathcal{J}_{br}$ based on* (20), (21), *and* (22) *using the partition $\mathcal{D}^m$ and metric* (4). *Let $X = (X_1, \ldots, X_n)$ be a general vector field where $X_i = (X_{p_i}, X_{E_i}) : Q \times \mathbb{R} \to \mathbb{R}^N \times \mathbb{R}$ for all $i \in \{1, \ldots, n\}$. Then, the Lie derivatives of $\mathcal{J}_{ea}$, $\mathcal{J}_a$, $\mathcal{J}_c$, $\mathcal{J}_m$, and $\mathcal{J}_{br}$ along the flow X are given by:*

$$\mathcal{L}_X \mathcal{J}_{ea} = \sum_{i=1}^{n} \frac{2M_i^m}{E_i^2}(C_i^m - p_i)^T X_{p_i} + \frac{2I_i^m}{E_i^3} X_{E_i}\,, \tag{31}$$

$$\mathcal{L}_X \mathcal{J}_a = \sum_{i=1}^{n} \left(\int_{\mathrm{Arcs}\left(D_i^m\right)} \phi(\gamma_i)[n^t(\gamma_i)]^T d\gamma_i \right) X_{p_i} + \left(\int_{\mathrm{Arcs}\left(D_i^m\right)} \phi(\gamma_i) d\gamma_i \right) X_{E_i}\,, \tag{32}$$

$$\mathcal{L}_X \mathcal{J}_c = \sum_{i=1}^{n} \left(\frac{2M_i^m}{E_i^2}(C_i^m - p_i)^T - \frac{\partial \mathcal{J}_a}{\partial p_i} \right) X_{p_i} + \left(\frac{2I_i^m}{E_i^3} - \frac{\partial \mathcal{J}_a}{\partial E_i} \right) X_{E_i}\,, \tag{33}$$

$$\mathcal{L}_X \mathcal{J}_m = \kappa_a \mathcal{L}_X \mathcal{J}_a + \kappa_c \mathcal{L}_X \mathcal{J}_c\,, \tag{34}$$

$$\mathcal{L}_X \mathcal{J}_{br} = \mathcal{L}_X \mathcal{J}_a + \sum_{i=1}^{n} \left[2\rho(q_o, p_i, E_i)(q_0 - p_i)^T \right] X_{p_i} + \left[2E_i \rho(q_o, p_i, E_i) \right] X_{E_i}\,. \tag{35}$$

Proof: Again, we will use the conservation of mass law in [11]. We will perform analysis of the objective functions (20), (21), and (22), and note that the gradient formulations for the remaining functions follow from those results.

Energy-aware (20). Similarly as in the proof of Proposition 4, we have that:

$$\begin{aligned}
\frac{\partial \mathcal{J}_{ea}}{\partial p_i} &= \sum_{j=1}^{n} \frac{\partial}{\partial p_i} \int_{V_j^m} -\frac{1}{E_j^2} \|q - p_j\|^2 \phi(q) dq \\
&= \sum_{j=1}^{n} \int_{V_j^m} -\frac{1}{E_j^2} \frac{\partial}{\partial p_i} \left[\|q - p_j\|^2 \right] \phi(q) dq + \int_{\partial V_j^m} -\frac{1}{E_j^2} \|\gamma_j - p_j\|^2 \phi(\gamma_j) n^t(\gamma_j) \frac{\partial \gamma_j}{\partial p_i} d\gamma_j \\
&= 2 \int_{V_i^m} \frac{1}{E_i^2} (q - p_i)^T \phi(q) dq + \sum_{j \in \mathcal{N}_i} \int_{\partial V_j^m} -\frac{1}{E_j^2} E_j^2 \phi(\gamma_j) n^t(\gamma_j) \frac{\partial \gamma_j}{\partial p_i} d\gamma_j \\
&= 2 \int_{V_i^m} \frac{1}{E_i^2} (q - p_i)^T \phi(q) dq\,.
\end{aligned}$$

Note that the integral along the boundaries ∂V_i^m vanish as in the power-weighted case. The energy derivative is:

$$\begin{aligned}\frac{\partial \mathcal{J}_{ea}}{\partial E_i} &= \sum_{j=1}^{n} \frac{\partial}{\partial E_i} \int_{V_j^m} -\frac{1}{E_j^2}\|q-p_j\|^2\phi(q)dq \\ &= \sum_{j=1}^{n} \int_{V_j^m} -\|q-p_j\|^2\phi(q)\frac{\partial}{\partial E_i}\left[\frac{1}{E_j^2}\right]dq + \int_{\partial V_j^m} -\frac{1}{E_j^2}\|\gamma_j-p_j\|^2\phi(\gamma_j)n^t(\gamma_j)\frac{\partial \gamma_j}{\partial E_i}d\gamma_j \\ &= 2\int_{V_i^m}\frac{1}{E_i^3}\|q-p_i\|^2\phi(q)dq + \sum_{j\in\mathcal{N}_i}\int_{\partial V_j^m} -\frac{1}{E_j^2}E_j^2\phi(\gamma_j)n^t(\gamma_j)\frac{\partial \gamma_j}{\partial E_i}d\gamma_j\,.\end{aligned}$$

Again, the integral along the boundaries vanish, giving the final result:

$$\frac{\partial \mathcal{J}_{ea}}{\partial p_i} = \frac{2M_i^m}{E_i^2}(C_i^m - p_i)^T\,, \quad \frac{\partial \mathcal{J}_{ea}}{\partial E_i} = \frac{2I_i^m}{E_i^3}\,.$$

Area coverage (21). The only difference between the objective functions (18) and (21) are the partitions. Thus, the analysis of the derivative is identical to the previous proof, with the exception of the different regions of integration, D_i^m as opposed to D_i^e.

Centroidal coverage (22). First take the derivative wrt p_i using conservation of mass law:

$$\begin{aligned}\frac{\partial \mathcal{J}_c}{\partial p_i} &= \sum_{j=1}^{n} \frac{\partial}{\partial p_i} \int_{D_j^m} -\frac{1}{E_j^2}\|q-p_j\|^2\phi(q)dq \\ &= \sum_{j=1}^{n} \int_{D_j^m} -\frac{1}{E_j^2}\frac{\partial}{\partial p_i}\left[\|q-p_j\|^2\right]\phi(q)dq + \int_{\partial D_j^m} -\frac{1}{E_j^2}\|\gamma_j-p_j\|^2\phi(\gamma_j)n^t(\gamma_j)\frac{\partial \gamma_j}{\partial p_i}d\gamma_j \\ &= 2\int_{D_i^m}\frac{1}{E_i^2}(q-p_i)^T\phi(q)dq + \sum_{j\in\mathcal{N}_i}\int_{\partial D_j^m} -\frac{1}{E_j^2}E_j^2\phi(\gamma_j)n^t(\gamma_j)\frac{\partial \gamma_j}{\partial p_i}d\gamma_j \\ &= 2\int_{D_i^m}\frac{1}{E_i^2}(q-p_i)^T\phi(q)dq - \int_{\mathrm{Arcs}\left(D_i^m\right)} n^t(\gamma_i)\phi(q)d\gamma_i \\ &= \frac{2M_i^m}{E_i^2}(C_i^m-p_i)^T - \frac{\partial \mathcal{J}_a}{\partial p_i}\,.\end{aligned}$$

The energy derivative follows similarly,

$$\begin{aligned}
\frac{\partial \mathcal{J}_c}{\partial E_i} &= \sum_{j=1}^{n} \frac{\partial}{\partial E_i} \int_{D_j^m} -\frac{1}{E_j^2}\|q-p_j\|^2\phi(q)dq \\
&= \sum_{j=1}^{n} \int_{D_j^m} -\|q-p_j\|^2\phi(q)\frac{\partial}{\partial E_i}\left[\frac{1}{E_j^2}\right]dq + \int_{\partial D_j^m} -\frac{1}{E_j^2}\|\gamma_j-p_j\|^2\phi(\gamma_j)n^t(\gamma_j)\frac{\partial \gamma_j}{\partial E_i}d\gamma_j \\
&= 2\int_{D_i^m} \frac{1}{E_i^3}\|q-p_i\|^2\phi(q)dq + \sum_{j\in\mathcal{N}_i}\int_{\partial D_j^m} -\frac{1}{E_j^2}E_j^2\phi(\gamma_j)n^t(\gamma_j)\frac{\partial \gamma_j}{\partial E_i}d\gamma_j \\
&= \frac{2I_i^m}{E_i^3} - \int_{\mathrm{Arcs}\left(D_i^m\right)} \|n^t(\gamma_i)\|^2\phi(\gamma_i)d\gamma_i = \frac{2I_i^m}{E_i^3} - \frac{\partial \mathcal{J}_a}{\partial E_i}\,.
\end{aligned}$$

■

Remark 7. In the area-maximizing case, $\mathcal{J}_a$, the gradient points in the direction that is the most "open". However, for the "centroidal" case, $\mathcal{J}_c$, there is a term which points in the opposite direction. For some choices of ϕ, this has a detrimental effect on coverage as seen through simulations. However, the mixed case, $\mathcal{J}_m$ with $\kappa_a = \kappa_c$ negates this effect, and the gradient direction points exactly towards the centroids, C_i^m, for all i. It seems that a more natural extension of the energy-aware case to the limited-range MWVD is $\mathcal{J}_m$ instead of $\mathcal{J}_c$. •

5. Gradient-ascent deployment algorithms

Once we have computed the gradient directions for each objective function, we will apply a gradient-ascent control algorithm for each case. The resulting control algorithms are extensions of Lloyd's algorithm for quantization [13], and are distributed in the sense of a (limited) Delaunay graph. Consider (1) with

$$\begin{aligned}
\dot{p}_i &= k(p_i, E_i)\,\mathrm{sat}\left(\frac{\partial \mathcal{F}}{\partial p_i}\right), \\
\dot{E}_i &= -\|\dot{p}_i\|^2\,,
\end{aligned} \tag{36}$$

for all $i \in \{1, \dots, n\}$, where the saturation function is

$$\text{sat}(v) = \begin{cases} v & , \|v\| \leq 1 \,, \\ \\ \frac{v}{\|v\|} & , \|v\| > 1 \,. \end{cases}$$

Here the control gain $k(p_i, E_i) \geq 0$ serves to modulate the velocity of each agent along its gradient climbing path.

Let $\mathcal{F}$ be any one of the objective functions analyzed in the previous section, with the exception of $\mathcal{J}_c$ as noted in Remark 7. Now we analyze the time evolution of the corresponding objective function $\mathcal{F}$ with respect to (36). We adopt the shorthand notation $k_i = k(p_i, E_i)$. Combining the gradient direction with the time derivatives above, we get the following time derivative:

$$\begin{aligned} \frac{d\mathcal{F}}{dt} &= \sum_{i=1}^{n} \frac{\partial \mathcal{F}}{\partial p_i} \dot{p}_i + \frac{\partial \mathcal{F}}{\partial E_i} \dot{E}_i = \sum_{i=1}^{n} k_i \frac{\partial \mathcal{F}}{\partial p_i} \cdot \text{sat}\left(\frac{\partial \mathcal{F}}{\partial p_i}\right) - k_i^2 \frac{\partial \mathcal{F}}{\partial E_i} \left\| \text{sat}\left(\frac{\partial \mathcal{F}}{\partial p_i}\right) \right\|^2 \\ &= \sum_{i=1}^{n} k_i \, \text{sat}\left(\frac{\partial \mathcal{F}}{\partial p_i}\right) \cdot \left(\frac{\partial \mathcal{F}}{\partial p_i} - k_i \frac{\partial \mathcal{F}}{\partial E_i} \, \text{sat}\left(\frac{\partial \mathcal{F}}{\partial p_i}\right) \right) . \end{aligned} \tag{37}$$

Remark 8. Non-smooth dynamics are also possible:

$$\dot{p}_i = k(p_i, E_i) \frac{\frac{\partial \mathcal{F}}{\partial p_i}}{\left\| \frac{\partial \mathcal{F}}{\partial p_i} \right\|} \,,$$

$$\dot{E}_i = -\|\dot{p}_i\|^2 = -k^2(p_i, E_i) \,.$$

Doing so would require the non-smooth analysis techniques found in [14]. We would, however, arrive at the same convergence conclusions found in the next subsections. •

Remark 9. The properties of the gradient of $\mathcal{F}$ as in Propositions 4 and 6 make the associated law (36) distributed in the sense of the corresponding Delaunay graph. For instance, with $\mathcal{F} = \mathcal{H}_a$, the law is distributed over $\mathcal{G}^e_{\text{LD}}$ because the information that an agent needs to implement (36) is only the position and energies of neighbors in $\mathcal{G}^e_{\text{LD}}$. With this information,

an agent can correctly construct its region, D_i^e. A sufficient condition to achieve this is if p_j can transmit to p_i when $\|p_i - p_j\| \leq 2E_m$ for all $j \neq i$. With this communication requirement, the control law described in (36) is spatially distributed over the graph $\mathcal{G}_{\text{LD}}^e$. •

5.1. Optimal gain selection

We wish that $\frac{d\mathcal{F}}{dt} \geq 0$ since we are maximizing the objective function. We now derive a sufficient condition for k and also present an optimal choice for k.

Lemma 10. *Given the model* (1), (36)*, and an objective function $\mathcal{F}$, the latter is maximized if*

$$0 \leq k(p_i, E_i) \leq \frac{\text{sat}\left(\frac{\partial \mathcal{F}}{\partial p_i}\right) \cdot \frac{\partial \mathcal{F}}{\partial p_i}}{\left\|\text{sat}\left(\frac{\partial \mathcal{F}}{\partial p_i}\right)\right\|^2 \frac{\partial \mathcal{F}}{\partial E_i}}\,, \tag{38}$$

for all $i \in \{1, \ldots, n\}$. An optimal choice of $k(p_i, E_i)$ is then

$$k^*(p_i, E_i) = \frac{1}{2} \frac{\text{sat}\left(\frac{\partial \mathcal{F}}{\partial p_i}\right) \cdot \frac{\partial \mathcal{F}}{\partial p_i}}{\left\|\text{sat}\left(\frac{\partial \mathcal{F}}{\partial p_i}\right)\right\|^2 \frac{\partial \mathcal{F}}{\partial E_i}}\,. \tag{39}$$

Proof: In order for $\frac{d\mathcal{F}}{dt} \geq 0$ we require that each summand of (37) be positive. Since $k(p_i, E_i) \geq 0$, we must have

$$\frac{\partial \mathcal{F}}{\partial p_i} \cdot \text{sat}\left(\frac{\partial \mathcal{F}}{\partial p_i}\right) - k_i \frac{\partial \mathcal{F}}{\partial E_i} \left\|\text{sat}\left(\frac{\partial \mathcal{F}}{\partial p_i}\right)\right\|^2 \geq 0\,.$$

Since $\frac{\partial \mathcal{F}}{\partial E_i} \geq 0$ in Propositions 4 and 6 (except for (33)), the formula in (38) follows.

We are free to choose k subject to (38). In particular, we would like to maximize each summand of (37) for each i. Taking the derivative with respect to k, we have

$$\frac{\partial \mathcal{F}}{\partial p_i} \cdot \text{sat}\left(\frac{\partial \mathcal{F}}{\partial p_i}\right) - 2k_i^* \frac{\partial \mathcal{F}}{\partial E_i} \left\|\text{sat}\left(\frac{\partial \mathcal{F}}{\partial p_i}\right)\right\|^2 = 0\,,$$

and the critical point condition for k_i follows. ■

Remark 11. Different energy dynamics can be considered. That is, the consideration of $g_i(x)$ different from x^2 is possible as long as $g_i(0) = 0$ and the g_i are sufficiently smooth.

Although using (39) provides the quickest rate of convergence, it may not be the best. Consider the situation shown in Figure 5, for the case where the objective function is (10). Agent 4 has a small arc component compared to its entire boundary. However with the area coverage gradient (24), the optimal gain (39) remains constant since $\frac{\partial \mathcal{H}_a}{\partial p_i}, \frac{\partial \mathcal{H}_a}{\partial E_i} \to 0$ at the same rate. For this reason, we would like k_i to be chosen by the following constrained optimization way: maximize each summand of (37) subject to $k_i \leq \frac{\partial \mathcal{F}}{\partial E_i}$. Notice that this quantity is of the form $f(k_i) = k_i(c_1 - k_i c_2)$, a concave parabola. With this constraint, the optimum k_i^* is then

$$k_i^* = \min \left\{ \frac{1}{2} \frac{\text{sat}\left(\frac{\partial \mathcal{F}}{\partial p_i}\right) \cdot \frac{\partial \mathcal{F}}{\partial p_i}}{\left\|\text{sat}\left(\frac{\partial \mathcal{F}}{\partial p_i}\right)\right\|^2 \frac{\partial \mathcal{F}}{\partial E_i}}, \frac{\partial \mathcal{F}}{\partial E_i} \right\}. \tag{40}$$

A simulation in Section 6 further discusses this choice.

For the PWVD energy-aware case, we can construct a similar constraint on k_i^*,

$$k_i^* = \min \left\{ \frac{1}{2} \frac{\text{sat}\left(\frac{\partial \mathcal{F}}{\partial p_i}\right) \cdot \frac{\partial \mathcal{F}}{\partial p_i}}{\left\|\text{sat}\left(\frac{\partial \mathcal{F}}{\partial p_i}\right)\right\|^2 \frac{\partial \mathcal{F}}{\partial E_i}}, \frac{E_i}{E_m} \right\}. \tag{41}$$

This choice of $\frac{E_i}{E_m}$ is motivated from [12]. With $k_i^* \leq \frac{E_i}{E_m}$, it can be shown that an individual agent will not run out of energy in finite time. For the MWVD case, this factor appears naturally in the optimal gain (39).

Similarly, we can impose a similar constraint for the base return flow such that if $\|p_i - q_0\| \leq E_i$, then the vehicle at p_i will always be able to return to q_0. We can choose

$$k_i^* = \min \left\{ \frac{1}{2} \frac{\text{sat}\left(\frac{\partial \mathcal{F}}{\partial p_i}\right) \cdot \frac{\partial \mathcal{F}}{\partial p_i}}{\left\|\text{sat}\left(\frac{\partial \mathcal{F}}{\partial p_i}\right)\right\|^2 \frac{\partial \mathcal{F}}{\partial E_i}}, 1 \right\}. \tag{42}$$

This is because when $k_i^* = 1$, $\|\dot{p}_i\| \leq 1$, which insures that a vehicle can reach any point in its travel range given in Section 2.

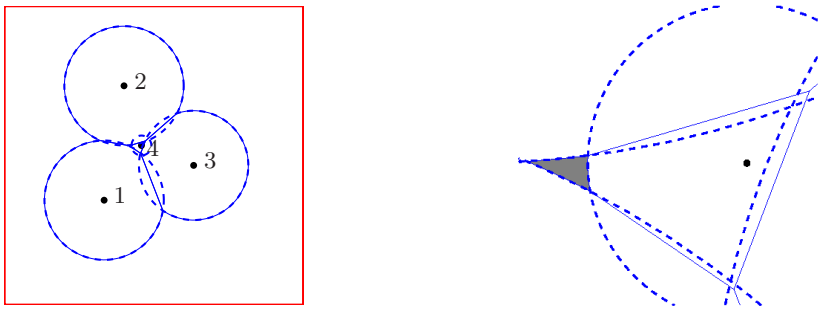

(a) (b)

Figure 5. Agent number 4 in (a), has a small arc component compared to its total boundary mass. The shaded area in (b) does not belong in the region of any agent. The energy radii, E_i, are shown as dotted lines.

5.2. Convergence analysis

We now replace the general objective, $\mathcal{H}$, with the functions developed in Section 4. The proof of the following theorem relies on the LaSalle invariance principle (see [15]).

Theorem 12 (Critical configurations and convergence, energy-aware PWVD) *The critical points of a gradient ascent flow characterized by* (36) *and appropriate choice of* k *using an objective function* $\mathcal{H}_{ea}$ *are configurations where each agent is either:*

(i) located at the centroid, $p_i = C_i^e$,

(ii) has an empty region, $V_i^e \cap Q = \emptyset$,

(iii) has no energy, $E_i = 0$.

Agents approach these critical configurations as $t \to \infty$.

Proof: From Lemma 10, $\frac{d\mathcal{F}}{dt} \geq 0$ using $\mathcal{F} = \mathcal{H}_{ea}$. Thus we need to characterize the critical points where $\frac{d\mathcal{H}_{ea}}{dt} = 0$. From (37), this is the case if for all $i \in \{1, \ldots, n\}$, either:

(i)

$$k_i = \min\left\{ \frac{1}{2} \frac{\text{sat}\left(\frac{\partial \mathcal{H}_{ea}}{\partial p_i}\right) \cdot \frac{\partial \mathcal{H}_{ea}}{\partial p_i}}{\left\|\text{sat}\left(\frac{\partial \mathcal{H}_{ea}}{\partial p_i}\right)\right\|^2 \frac{\partial \mathcal{H}_{ea}}{\partial E_i}}, \frac{E_i}{E_m} \right\} = 0\,, \tag{43}$$

(ii)

$$\text{sat}\left(\frac{\partial \mathcal{H}_{ea}}{\partial p_i}\right) = \text{sat}\left(2M_i^e (C_i^e - p_i)^T\right) = 0\,, \tag{44}$$

(iii) or

$$\frac{\partial \mathcal{H}_{ea}}{\partial p_i} - k_i \frac{\partial \mathcal{H}_{ea}}{\partial E_i} \text{sat}\left(\frac{\partial \mathcal{H}_{ea}}{\partial p_i}\right) = 0\,. \tag{45}$$

Case (43) implies either $\frac{\partial \mathcal{H}_{ea}}{\partial p_i} = 0$ or $E_i = 0$. Case (44) also implies that $\frac{\partial \mathcal{H}_{ea}}{\partial p_i} = 0$, which occurs if either $M_i^e = 0$ or $p_i = C_i^e$. The case where $M_i^e = 0$ implies that the region $V_i^e \cap Q = \emptyset$.

To analyze case (45), we consider a situation when $\left\|\frac{\partial \mathcal{H}_{ea}}{\partial p_i}\right\| \leq 1$ and when $\left\|\frac{\partial \mathcal{H}_{ea}}{\partial p_i}\right\| > 1$. For the former case,

$$\frac{\partial \mathcal{H}_{ea}}{\partial p_i}\left[1 - \min\left\{\frac{1}{2\frac{\partial \mathcal{H}_{ea}}{\partial E_i}}, \frac{E_i}{E_m}\right\}\frac{\partial \mathcal{H}_{ea}}{\partial E_i}\right] = 0\,,$$

$$\frac{\partial \mathcal{H}_{ea}}{\partial p_i}\left[1 - \min\left\{\frac{1}{2}, \frac{E_i}{E_m}\frac{\partial \mathcal{H}_{ea}}{\partial E_i}\right\}\right] = 0\,.$$

This implies that $\frac{\partial \mathcal{H}_{ea}}{\partial p_i} = 0$, a case addressed in (44) (the quantity $1 - \min\left\{\frac{1}{2}, \frac{E_i}{E_m}\frac{\partial \mathcal{H}_{ea}}{\partial E_i}\right\}$ cannot be zero). The latter case, when $\left\|\frac{\partial \mathcal{H}_{ea}}{\partial p_i}\right\| > 1$ leads to:

$$\frac{\partial \mathcal{H}_{ea}}{\partial p_i}\left[1 - \min\left\{\frac{\left\|\frac{\partial \mathcal{H}_{ea}}{\partial p_i}\right\|}{2\frac{\partial \mathcal{H}_{ea}}{\partial E_i}}, \frac{E_i}{E_m}\right\}\frac{\frac{\partial \mathcal{H}_{ea}}{\partial E_i}}{\left\|\frac{\partial \mathcal{H}_{ea}}{\partial p_i}\right\|}\right] = 0\,,$$

$$\frac{\partial \mathcal{H}_{ea}}{\partial p_i}\left[1 - \min\left\{\frac{1}{2}, \frac{E_i}{E_m}\frac{\frac{\partial \mathcal{H}_{ea}}{\partial E_i}}{\left\|\frac{\partial \mathcal{H}_{ea}}{\partial p_i}\right\|}\right\}\right] = 0\,.$$

This again implies that $\frac{\partial \mathcal{H}_{ea}}{\partial p_i} = 0$, addressed earlier (the quantity in the brackets cannot be zero).

We now characterize the invariant configurations, when $\dot{p}_i = 0$ for all $i \in \{1, \ldots, n\}$. This corresponds to the cases (43) and (44). The largest invariant set contained in $S =$

$\{(p_1, \ldots, p_n) \mid \dot{\mathcal{H}}_{ea} = 0\}$ is S itself. By the LaSalle invariance principle, system configurations will asymptotically approach S. ■

Theorem 13 (Critical configurations and convergence, energy-limited PWVD) *The critical points of a gradient ascent flow characterized by* (36) *and appropriate choice of* k *using an objective function* $\mathcal{H} \in \{\mathcal{H}_a, \mathcal{H}_c, \mathcal{H}_m, \mathcal{H}_{br}\}$ *are configurations where each agent either satisfies* $\frac{\partial \mathcal{H}}{\partial p_i} = 0$*, or its region* $D_i^e = \emptyset$*. The statement* $\frac{\partial \mathcal{H}}{\partial p_i} = 0$ *has the following meanings:*

(i) the vehicle cannot further locally increase its coverage area when using $\mathcal{H}_a$*,*

(ii) vehicle i *is located at the centroid of* D_i^e *when using* $\mathcal{H}_c$*,*

(iii) the vehicle has reached a balance between maximizing area covered and remaining close to the centroid of D_i^e *when using* $\mathcal{H}_m$*, and*

(iv) the vehicle has reached a balance between maximizing area covered and remaining close to the point q_0 *when using* $\mathcal{H}_{br}$*.*

Agents approach these critical configurations as $t \to \infty$*.*

Proof: The results for each deployment objective function will follow from the LaSalle invariance principle; see [15]. We will present the proof for the Area coverage objective function (18) and note that the proofs for the remaining cases are similar.

The region Q is positively invariant since agents cannot leave it. Also, using k_i^* from (40) into (37) results in $\dot{\mathcal{H}}_a \geq 0$ in Q. We now compute the critical points where $\dot{\mathcal{H}}_a = 0$. From (37), this occurs when either $k_i^* = 0$, or $\text{sat}\left(\frac{\partial \mathcal{H}_a}{\partial p_i}\right) = 0$, or when

$$\left(\frac{\partial \mathcal{H}_a}{\partial p_i} - k_i^* \frac{\partial \mathcal{H}_a}{\partial E_i} \,\text{sat}\left(\frac{\partial \mathcal{H}_a}{\partial p_i}\right)\right) = 0\,, \tag{46}$$

for all $i \in \{1, \ldots, n\}$.

If $k_i^* = 0$, we divide the problem into the case where $\left\| \frac{\partial \mathcal{H}_a}{\partial p_i} \right\| \leq 1$ or where $\left\| \frac{\partial \mathcal{H}_a}{\partial p_i} \right\| > 1$. If the former is true, then

$$k_i^* = \min \left\{ \frac{1}{2\frac{\partial \mathcal{H}_a}{\partial E_i}}, \frac{\partial \mathcal{H}_a}{\partial E_i} \right\} = 0 \,.$$

since $\frac{\partial \mathcal{H}_a}{\partial E_i}$ is bounded, then $\frac{\partial \mathcal{H}_a}{\partial E_i} = 0$. If $\left\| \frac{\partial \mathcal{H}_a}{\partial p_i} \right\| > 1$,

$$k_i^* = \min \left\{ \frac{\left\| \frac{\partial \mathcal{H}_a}{\partial p_i} \right\|}{2\frac{\partial \mathcal{H}_a}{\partial E_i}}, \frac{\partial \mathcal{H}_a}{\partial E_i} \right\} = 0 \,,$$

and either $\frac{\partial \mathcal{H}_a}{\partial p_i} = 0$ or $\frac{\partial \mathcal{H}_a}{\partial E_i} = 0$. This implies that either

$$\int_{\text{Arcs}\left(D_i^e\right)} \phi(\gamma_i)[n^t(\gamma_i)]^T d\gamma_i = 0 \text{ or } \int_{\text{Arcs}\left(D_i^e\right)} \phi(\gamma_i) d\gamma_i = 0 \,.$$

Assuming that $\phi \neq 0$ in Q, the first equation implies that either $\text{Arcs}\,(D_i^e) = \emptyset$ or that the integral over the boundary is balanced in all directions. The latter equation also implies that $\text{Arcs}\,(D_i^e) = \emptyset$. This occurs if either $E_i = 0$, or D_i^e is composed entirely of Voronoi edges (the boundary of Q counts as a Voronoi edge), or $D_i^e = \emptyset$.

Now suppose that (46) is true. When $\text{sat}\left(\frac{\partial \mathcal{H}_a}{\partial p_i}\right) = 0$, this implies that $\frac{\partial \mathcal{H}_a}{\partial p_i} = 0$, and we have addressed this situation. When (46) is true, we substitute (40) into (46) and consider the case where $\left\| \frac{\partial \mathcal{H}_a}{\partial p_i} \right\| \leq 1$ or where $\left\| \frac{\partial \mathcal{H}_a}{\partial p_i} \right\| > 1$. When the former is true,

$$\begin{aligned} &\frac{\partial \mathcal{H}_a}{\partial p_i} - \min \left\{ \frac{1}{2\frac{\partial \mathcal{H}_a}{\partial E_i}}, \frac{\partial \mathcal{H}_a}{\partial E_i} \right\} \frac{\partial \mathcal{H}_a}{\partial E_i} \left(\frac{\partial \mathcal{H}_a}{\partial p_i} \right) = 0 \\ &\quad \Longrightarrow \quad \frac{\partial \mathcal{H}_a}{\partial p_i} \left[1 - \min \left\{ \frac{1}{2}, \left(\frac{\partial \mathcal{H}_a}{\partial E_i} \right)^2 \right\} \right] = 0 \,, \end{aligned}$$

which implies $\frac{\partial \mathcal{H}_a}{\partial p_i} = 0$ or $1 = \min \left\{ \frac{1}{2}, \left(\frac{\partial \mathcal{H}_a}{\partial E_i} \right)^2 \right\}$, a contradiction. Similarly $\left\| \frac{\partial \mathcal{H}_a}{\partial p_i} \right\| > 1$, implies $\frac{\partial \mathcal{H}_a}{\partial p_i} = 0$. For both cases we conclude that $\frac{\partial \mathcal{H}_a}{\partial p_i} = 0$, a situation that we have addressed earlier.

We now characterize the set of invariant configurations. The system is positively invariant if $\dot{p}_i = 0$ for all $i \in \{1, \ldots, n\}$. From (36), this occurs when $k_i^* = 0$ or $\text{sat}\left(\frac{\partial \mathcal{H}_a}{\partial p_i}\right) = 0$ for all

$i \in \{1, \ldots, n\}$. Therefore, the invariant configurations are exactly where $\dot{\mathcal{H}}_a = 0$, which have been described. By LaSalle's invariance principle [15], the agents will asymptotically approach this set of configurations. ■

Next we present the analogous result for coverage control using partitions based on the MWVD. However, we omit the results of using $\mathcal{J}_c$ (22) for reasons stated in Remark 7.

Theorem 14 (Critical configurations and convergence, energy-aware MWVD) *The critical points of a gradient ascent flow characterized by* (36) *and appropriate choice of k using an objective function $\mathcal{J}_{ea}$ are configurations where each agent is either:*

(i) located at the centroid, $p_i = C_i^e$,

(ii) has no energy, $E_i = 0$.

Agents approach these critical configurations as $t \to \infty$.

Proof: The proof is similar to that of Theorem 12. ■

Theorem 15 (Critical configurations and convergence, energy-limited MWVD) *The critical points of a gradient ascent flow characterized by* (36) *and appropriate choice of k using an objective function $\mathcal{J} \in \{\mathcal{J}_a, \mathcal{J}_m, \mathcal{J}_{br}\}$ are configurations where each agent either satisfies $\frac{\partial \mathcal{J}}{\partial p_i} = 0$, or has no energy, $E_i = 0$. The statement $\frac{\partial \mathcal{J}}{\partial p_i} = 0$ has the following meanings:*

(i) the vehicle cannot further locally increase its coverage area when using $\mathcal{J}_a$,

(ii) the vehicle has reached the centroid of D_i^m when using $\mathcal{J}_m$, and

(iii) the vehicle has reached a balance between maximizing area covered and remaining close to the point q_0 when using $\mathcal{J}_{br}$.

Agents approach these critical configurations as $t \to \infty$.

Proof: The proof is similar to that of Theorem 13. ■

6. Simulations

In this section, we present simulation results for the three coverage objectives. First, however, we will address the motivation for choosing k_i^* from (40) over (39). In this simulation, $n = 8$ agents were initialized at random initial positions with $E_i = 10$ for $i \in \{1, \ldots, 8\}$. The agents were confined to $Q = [0, 15] \times [0, 15] \subset \mathbb{R}^2$ with $\phi(x, y) = 1 + 10 \exp[-\frac{1}{9}((x-10)^2 + (y-10)^2)]$. The agents maximized the area coverage objective function (10).

The use of k_i^* from (40) demonstrates some advantages over (39) in the simulation of Figure 6. In Figure 6(a), agent 4 finishes with almost no energy, while the same agent has significantly more energy in Figure 6(b). In addition, all 8 agents were deployed in Figure 6(a) while only 5 agents left the starting location in Figure 6(b).

We now compare the performance between deployment algorithms based on the PWVD versus the MWVD. Specifically, we will look at the performance of energy-aware deployment $\mathcal{H}_{ea}$ and $\mathcal{J}_{ea}$, area maximizing deployment $\mathcal{H}_a$ and $\mathcal{J}_a$, mixed coverage deployment $\mathcal{H}_m$ and $\mathcal{J}_m$, and base-return coverage $\mathcal{H}_{br}$ and $\mathcal{J}_{br}$.

6.1. Energy-aware coverage case

Here, $n = 12$ agents are confined to $Q = [0, 10] \times [0, 10] \subset \mathbb{R}^2$ with a density function ϕ composed of 4 Gaussian distributions (see Figure 7). The density function used was

$$\phi(q) = 1 + 10 \left[e^{-\frac{\|q-r_1\|^2}{9}} + e^{-\frac{\|q-r_2\|^2}{2}} + e^{-\frac{\|q-r_3\|^2}{2}} + e^{-\|q-r_4\|^2} \right],$$

where $r_1 = (8, 8)$, $r_2 = (8, 2)$, $r_3 = (8, 4)$ and $r_4 = (3, 7)$. Agents started at random positions in the lower-left corner, with $E_i = 5$ for $i \in \{1, \ldots, 12\}$. The agents followed the gradient ascent

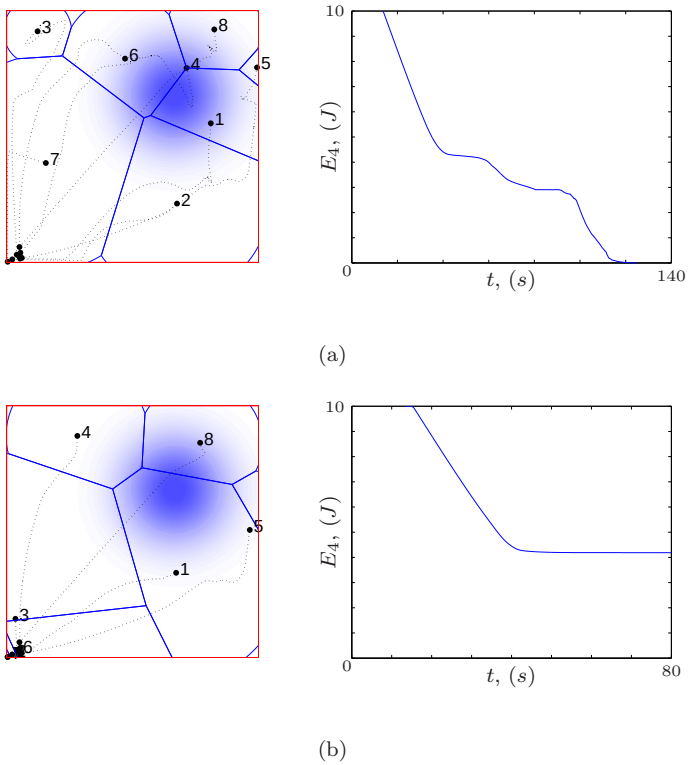

Figure 6. Comparison between the performance of k_i^* from (39), (a); and from (40), (b). Agent paths and final configurations are shown at left, and the energy level of agent 4 is plotted at right. Shaded regions indicate a high value of ϕ.

control law in (36), and used (40).

Remark 16. Because it is possible for an agent i to be outside of its region of dominance V_i^e, i.e.: $p_i \notin V_i^e$, it is oftentimes the case where $V_i^e \cap Q = \emptyset$ when p_i is close to the boundary of Q, and $E_i < E_j$ for $j \in \mathcal{N}_i^e$ This phenomena can be observed in the simulation of Figure 7 (left). From an energy perspective, the use of these sensors is wasted, since they are pushed away and don't play any role in the coverage task. This raises the question of how to characterize the number of sensors needed to cover a given region under the PWVD-based algorithms.

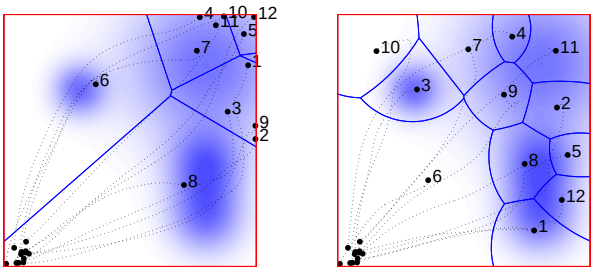

Figure 7. Energy-aware coverage simulation results. Shaded regions indicate a high value of ϕ. The path lines and final configurations are shown for energy-aware PWVD coverage (17), left, and energy-aware MWVD coverage (20), right.

The undesirable behavior of the PWVD energy-aware algorithm is avoided when using the MWVD based algorithm, since it is a property of the MWVD that $p_i \in V_i^m$. In this regard, the MWVD forces the participation of all sensors in the coverage task. The use of the PWVD would require an assessment of how many sensors are enough to solve the coverage task.

6.2. Area coverage case

We now examine the area coverage case, (18) and (21). The system of agents was initialized identically to the energy-aware simulations, and we compare the performance between the PWVD-based deployment and the MWVD-based deployment.

Here we do not see the undesirable effect in the PWVD case (Figure 8, left) of agents lying along the boundary of Q without a region of dominance. This is because the gradient, $\frac{\partial \mathcal{H}_a}{\partial p_i}$ tends to zero as $\mathrm{Arcs}\,(D_i^e)$ disappear, preventing agents from getting squeezed into the boundary. Both algorithms perform similarly, deploying to cover almost all of Q in both cases.

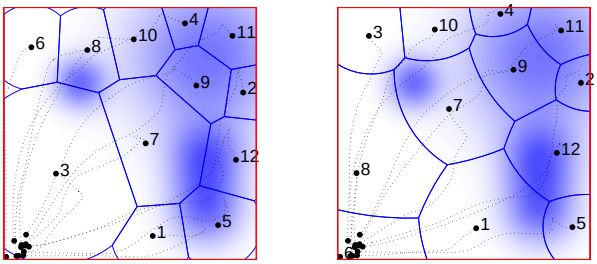

Figure 8. Area coverage simulation results. The path lines and final configurations are shown for limited-range PWVD area coverage (18), left, and limited-range MWVD area-coverage (21), right.

6.3. Mixed coverage case

The third simulation presents the mixed-coverage cases, $\mathcal{H}_m$ and $\mathcal{J}_m$ with identical initial conditions as before. The area and centroidal components carried equal weight, $\kappa_a = \kappa_c = 1$ from (12).

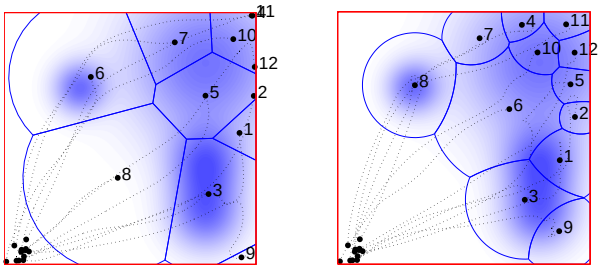

Figure 9. Mixed coverage simulation results. The path lines and final configurations are shown for limited-range PWVD mixed coverage $\mathcal{H}_m$, left, and limited-range MWVD mixed coverage $\mathcal{J}_m$, right.

We again notice the return of the same undesirable phenomena mentioned in the energy-aware simulations for the energy-limited PWVD simulation in Figure 10, left. Despite this, the mixed coverage algorithm resulted in agent positions that are more collocated with dense regions of ϕ for both the PWVD and MWVD cases, as compared to Figure 8.

6.4. Base return coverage case

In this third simulation we examine the performance of $\mathcal{H}_{br}$ and $\mathcal{J}_{br}$ with $\rho(q_0, p_i, E_i) = -\exp[\|q_0 - p_i\|^2 - E_i^2]$ and $q_0 = (0, 0)$. Agents remain in $Q = [-5, 5] \times [-5, 5] \subset \mathbb{R}^2$ and $\phi(x, y) = 1$. We initialized $n = 8$ agents randomly around the origin with $E_i = 3$ for all $i \in \{1, \ldots, 8\}$, and agents used k_i^* from (42).

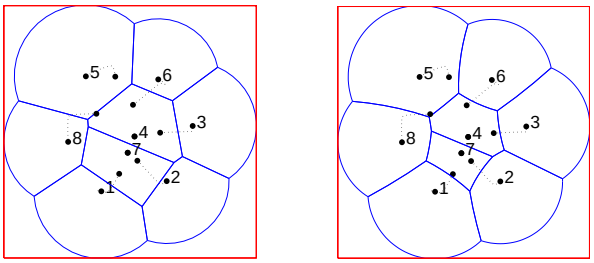

Figure 10. Base-return coverage simulation results. The path lines and final configurations are shown for limited-range PWVD case $\mathcal{H}_{br}$, left, and limited-range MWVD case $\mathcal{J}_{br}$, right.

The simulations have almost identical results, with the exception of different partitioning schemes. The agents manage to stay close enough to the origin when fully deployed.

7. Conclusions

We have presented a novel set of spatially distributed coverage control algorithms. We designed three objective functions to demonstrate the flexibility of this method. In addition each of these algorithms place an emphasis on individual energy levels through use of a generalized Voronoi partition. We have shown through simulation that the three cases that we developed perform as intended.

Current work includes incorporating nonholonomic vehicle dynamics into the convergence

analysis in order to provide a more practical coverage scenario for implementation in a physical testbed. Since the convergence of the algorithms is only guaranteed to local optima, we are also working on extensions that help us find more optimal coverage configurations.

REFERENCES

1. Estrin D, Culler D, Pister K, Sukhatme G. Connecting the physical world with pervasive networks. *IEEE Pervasive Computing* 2002; **1**(1):59–69.
2. Cortés J, Martínez S, Karatas T, Bullo F. Coverage control for mobile sensing networks. *IEEE Transactions on Robotics and Automation* 2004; **20**(2):243–255.
3. Howard A, Matarić MJ, Sukhatme GS. Mobile sensor network deployment using potential fields: A distributed scalable solution to the area coverage problem. *International Conference on Distributed Autonomous Robotic Systems (DARS02)*, Fukuoka, Japan, 2002; 299–308.
4. Poduri S, Sukhatme GS. Constrained coverage for mobile sensor networks. *IEEE Int. Conf. on Robotics and Automation*, 2004; 165–172.
5. Raghunathan V, Pereira C, Srivastava M, Gupta R. Energy-aware wireless systems with adaptive power-fidelity tradeoffs. *IEEE Trans. Very Large Scale Integration Systems* February 2005; **13**(2):211–225.
6. Mohapatra S, Dutt N, Nicolau A, Venkatasubramanian N. DYNAMO: A cross-layer framework for end-to-end QoS and Energy Optimization in Mobile Handheld Devices. *IEEE J. Selected Areas in Communication* May 2007; .
7. Heo N, Varshney PK. Energy-efficient deployment of intelligent mobile sensor networks. *IEEE Transactions on Systems, Man and Cybernetics, Part A* January 2005; **35**(1):78–92.
8. Wang G, Cao G, Porta TL. Movement-assisted sensor deployment. *IEEE Transactions on Mobile Computing* June 2006; :640–652.
9. Mei Y, Lu Y, Hu Y, Lee C. Deployment of mobile robots with energy and timing constraints. *IEEE Transactions on Robotics and Automation* June 2006; **22**(3):507–522.
10. Okabe A, Boots B, Sugihara K, Chiu SN. *Spatial Tessellations: Concepts and Applications of Voronoi Diagrams*. 2 edn., Wiley Series in Probability and Statistics, John Wiley: New York, 2000.
11. Cortés J, Martínez S, Bullo F. Spatially-distributed coverage optimization and control with limited-range interactions. *ESAIM. Control, Optimisation & Calculus of Variations* 2005; **11**:691–719.

12. Kwok A, Martínez S. Energy-balancing cooperative strategies for sensor deployment. *IEEE International Conference on Decision and Control*, New Orleans, USA, 2007; 6136–6141.
13. Lloyd SP. Least squares quantization in PCM. *IEEE Transactions on Information Theory* 1982; **28**(2):129–137. Presented as Bell Laboratory Technical Memorandum at a 1957 Institute for Mathematical Statistics meeting.
14. Cortés J. Finite-time convergent gradient flows with applications to network consensus. *Automatica* November 2006; **42**(11):1993–2000.
15. Khalil HK. *Nonlinear Systems*. 3 edn., Prentice Hall, 2001.